The Journal of Experimental Biology 215, 4196-4207

doi:10.1242/jeb.076513

RESEARCH ARTICLE

Beyond the Jamming Avoidance Response: weakly electric fish respond to the envelope of social electrosensory signals

Sarah A. Stamper[1,*,†], Manu S. Madhav[2,†], Noah J. Cowan[2] and Eric S. Fortune[2,3]

[1]Department of Psychological and Brain Sciences and [2]Department of Mechanical Engineering, Johns Hopkins University, Baltimore, MD 21218, USA and [3]Department of Biological Sciences, New Jersey Institute of Technology, Newark, NJ 07102, USA

*Author for correspondence (sstamper@jhu.edu)
†These authors contributed equally to this work

SUMMARY

Recent studies have shown that central nervous system neurons in weakly electric fish respond to artificially constructed electrosensory envelopes, but the behavioral relevance of such stimuli is unclear. Here we investigate the possibility that social context creates envelopes that drive behavior. When *Eigenmannia virescens* are in groups of three or more, the interactions between their pseudo-sinusoidal electric fields can generate 'social envelopes'. We developed a simple mathematical prediction for how fish might respond to such social envelopes. To test this prediction, we measured the responses of *E. virescens* to stimuli consisting of two sinusoids, each outside the range of the Jamming Avoidance Response (JAR), that when added to the fish's own electric field produced low-frequency (below 10 Hz) social envelopes. Fish changed their electric organ discharge (EOD) frequency in response to these envelopes, which we have termed the Social Envelope Response (SER). In 99% of trials, the direction of the SER was consistent with the mathematical prediction. The SER was strongest in response to the lowest initial envelope frequency tested (2 Hz) and depended on stimulus amplitude. The SER generally resulted in an increase of the envelope frequency during the course of a trial, suggesting that this behavior may be a mechanism for avoiding low-frequency social envelopes. Importantly, the direction of the SER was not predicted by the superposition of two JAR responses: the SER was insensitive to the amplitude ratio between the sinusoids used to generate the envelope, but was instead predicted by the sign of the difference of difference frequencies.

Key words: *Eigenmannia*, electrosensory system, second-order statistics.

Received 12 July 2012; Accepted 26 August 2012

INTRODUCTION

Weakly electric fish generate an electric organ discharge (EOD) that results in an electric field that surrounds the fish's body. In *Eigenmannia*, the EOD is quasi-sinusoidal and when fish are in close proximity (~1 m or less) their EODs interact. In the case of two nearby conspecifics, the combined EOD signal has a modulation, termed the amplitude modulation (AM). If there are more than two nearby conspecifics or relative movements between conspecifics, the combined EOD signal contains modulations of the AM, which has been termed the electrosensory envelope (Middleton et al., 2006).

The interactions of two EODs have been well studied in relation to the Jamming Avoidance Response (JAR). When two nearby conspecifics have EOD signals S_1 and S_2 at frequencies of f_1 and f_2, respectively, the combined signal, S_1+S_2, has an emergent AM. The AM frequency is at the frequency difference, $|df|$, where $df=f_2-f_1$. When two neighboring *Eigenmannia* have EODs of similar frequency (e.g. 500 and 505 Hz, with $|df|=5$ Hz) they perform the JAR, during which each fish will raise or lower their individual EOD frequency to increase $|df|$, and thus the AM frequency.

When there are three or more EOD signals it is possible that fish are responding not only to the AM but also to the emergent envelope. Here we define a 'social envelope' as the modulation of the AM that occurs when at least three EODs are added. For example, if there are three EOD signals, S_1, S_2 and S_3, at frequencies f_1, f_2 and f_3, respectively, the combined signal $S_1+S_2+S_3$ can have an AM; the magnitude of this AM also fluctuates over time, referred to here as the envelope of the AM (Fig. 1A) (see Appendix, Definition of envelopes). Thus, it is possible that even with high $|df|$ values there could be a low-frequency envelope (as shown in Fig. 1).

Understanding the behavioral relevance and sensory processing of envelope information has proven challenging in part because the extraction of envelope information requires nonlinear processing (Fig. 1B; see Appendix, Methods for envelope extraction). However, recent neurophysiological studies have already identified envelope-related neural activity at each level from the receptor afferents to the midbrain in weakly electric fish (Middleton et al., 2006; Middleton et al., 2007; Longtin et al., 2008; Savard et al., 2011; McGillivray et al., 2012), suggesting that not only can the fish extract envelope information but there might also be behavioral relevance of these signals for the animals.

Model-based prediction of the Social Envelope Response

The beauty of the JAR is that the behavioral response can be predicted based on a simple algorithm (Heiligenberg, 1991). For the fish to shift its EOD frequency in the 'correct' direction (e.g. the direction that increases $|df|$), the fish must be able to compute the sign of the df. The fish does this without an efference copy of its own EOD (Bullock et al., 1972) using amplitude and phase

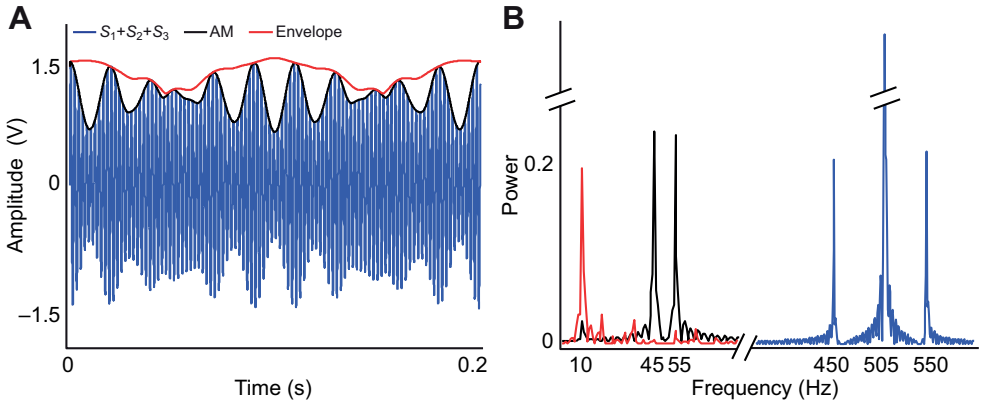

Fig. 1. Social electrosensory envelopes. (A) A signal composed of three sinusoids added together (blue) at frequencies of 505 (S_1), 450 (S_2) and 550 Hz (S_3). The interactions of these stimuli create an amplitude modulation (AM; black), which can be extracted from the signal using a Hilbert transform. Because the S_1 amplitude is larger than the amplitude of S_2 and S_3, a well-defined envelope emerges (red) that can be extracted from the AM using a Hilbert transform. (B) Power spectra of the signal (blue), the AM (black) and the envelope (red). The two peaks of the AM correspond to the |df| values at 45 and 55 Hz and the peak of the envelope corresponds to the |dd$f$| at 10 Hz.

modulation information measured across the body (e.g. multiple electroreceptors) (Metzner, 1999).

The JAR computation is diagrammatically represented as a Lissajous figure in the amplitude-phase plane (Fig. 2A), which was pioneered by Heiligenberg and Bastian (Heiligenberg and Bastian, 1980) and has been verified through electrophysiological recordings (Bastian and Heiligenberg, 1980). The plot is the magnitude (x-axis) *versus* the phase (y-axis) of the complex representation of the combined signal (see Appendix, The amplitude-phase Lissajous). The Lissajous trajectory will rotate clockwise for negative df and counter-clockwise for positive df at a frequency of |df|. The direction of rotation of the Lissajous predicts the direction that the fish will shift its EOD during the JAR.

When three sinusoids (or EODs) interact, AMs emerge at each of the |df| values, and the Lissajous is more complicated (Fig. 2B). For example, if there are three EOD signals, S_1, S_2 and S_3, at frequencies f_1, f_2 and f_3, there will be AMs at the magnitudes of the following df values: $df_2=f_2-f_1$, $df_3=f_3-f_1$ and $df_1=f_3-f_2$. However, the signal measured by each fish is typically dominated by its own EOD. So, for fish 1 the signal S_1 dominates the others (S_2 and S_3) and correspondingly, the AMs at $|df_2|$ and $|df_3|$ dominate the AM at $|df_1|$. In this case, the AM at $|df_1|$ can be considered negligible, and the dominant envelope frequency emerges at $dd f=|df_3|-|df_2|$ (see Eqn A18). Note that dd$f$ is a signed quantity, which is important to the predictions stated below.

In this paper, we hypothesize that the JAR circuit can be extended to predict a behavioral response to signals outside the range of the JAR that nevertheless generate low-frequency envelopes. In some cases, two conspecific signals (S_2 and S_3) when added to S_1 produce a low-frequency envelope (see Appendix, Caveats of the analytic signal method). Two such cases are depicted in Fig. 2B – positive and negative dd$f$. At first glance, the 'floral' pattern of the Lissajous seems to lack a consistent rotation. However, each of the 'petals'

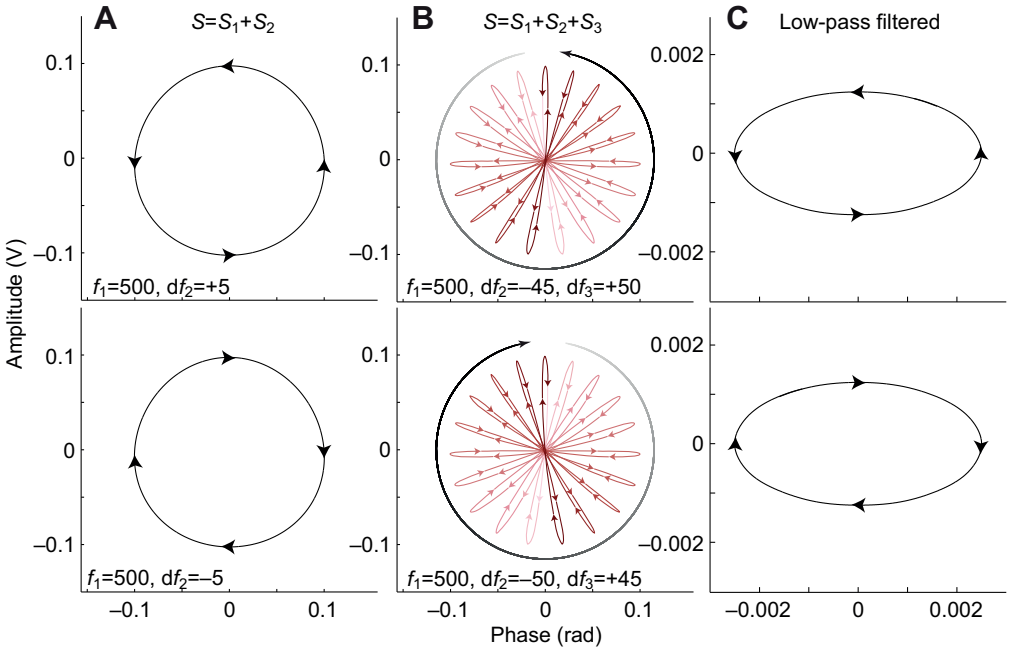

Fig. 2. Amplitude-phase Lissajous of two or three sinusoidal signals. (A) The sum of two signals S_1 and S_2 produces a circular graph that rotates counter-clockwise for positive df (top) and clockwise for negative df (bottom), at frequency |df|. (B) The sum of three signals S_1, S_2 and S_3 results in a more complex Lissajous figure, for positive dd$f$ (top) and negative dd$f$ (bottom). The Lissajous has a local rotation (arrows on petals) and also a general precession (external arrow and increasing color gradient on petals) (C) The amplitude and phase from B were low-pass filtered (Butterworth, sixth-order, 20 Hz normalized cut-off). This shows that there is a low-frequency precession of the graph in the counter-clockwise direction for positive dd$f$ (top) and clockwise for negative dd$f$ (bottom). The precession is at frequency |dd$f$|.

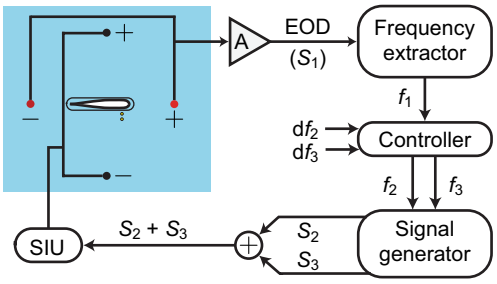

Fig. 3. The fish's EOD is recorded *via* head–tail electrodes (red circles) and amplified (A). Stimuli to the fish are applied *via* transverse electrodes (black circles). Stimuli consist of a single sinusoid (S_2) or a sum of two sinusoids (S_2+S_3). The frequency of the recorded EOD is extracted (f_1), and a controller adds the stimulus values of df_2 and df_3 to f_1 to produce output frequencies f_2 and f_3, respectively. The signal generator produces sinusoids S_2 and S_3 at frequencies f_2 and f_3. S_2 and S_3 are added, and applied to the tank through a stimulus isolation unit (SIU). A dipole (small yellow circles) was used to measure the local electric field.

precesses in a direction corresponding to the sign of the dd*f*, at frequency |dd*f*| (see Appendix, The amplitude-phase Lissajous). Upon low-pass filtering of both the amplitude and phase signals, the petals are filtered out and the general, slow precession emerges (Fig. 2C).

Interestingly, as the amplitude ratio between the signals is inverted, the direction of rotation of individual petals flips, but the direction of the precession remains unchanged. Does the fish respond to the direction of the petals (d*f* values and amplitude ratio) or the precession (dd*f*)? When the d*f* values are within the JAR range the response of the fish follows the petals (Partridge and Heiligenberg, 1980). But what happens when the d*f* values are outside the JAR range? We hypothesize that fish respond to the emergent envelope at the |dd*f*|, governed by the precession as revealed by the low-pass filtered model (see Appendix, The amplitude-phase Lissajous). If, as our model predicts, the fish uses a downstream low-pass filter from the JAR circuit to extract envelope information, it could drive a behavioral Social Envelope Response (SER), much like the JAR to AM stimuli.

MATERIALS AND METHODS

Adult *Eigenmannia virescens* (Valenciennes 1836) (10–15 cm in length) were obtained through a commercial vendor and housed in aquarium tanks with a water temperature of ~27°C and conductivity in the range of 150–300 μS cm^{-1} (Hitschfeld et al., 2009). All fish used in these experiments were housed in social tanks that contained two to five individuals. These experiments were conducted at the Johns Hopkins University between 2009 and 2012. All experimental procedures were approved by the Johns Hopkins Animal Care and Use Committee and followed guidelines established by the National Research Council and the Society for Neuroscience.

Experimental procedure

Each individual fish (N=4) was transferred to the testing tank (27±1°C and 175±25 μS cm^{-1}) and allowed to acclimate for 2–12 h before experiments began. During the acclimation period a second fish was also in the testing tank, to provide recent social experience, but was removed before the start of the experiment. For testing, the experimental fish was restricted in a chirp chamber to prevent movement. Experiments were started when the EOD frequency did

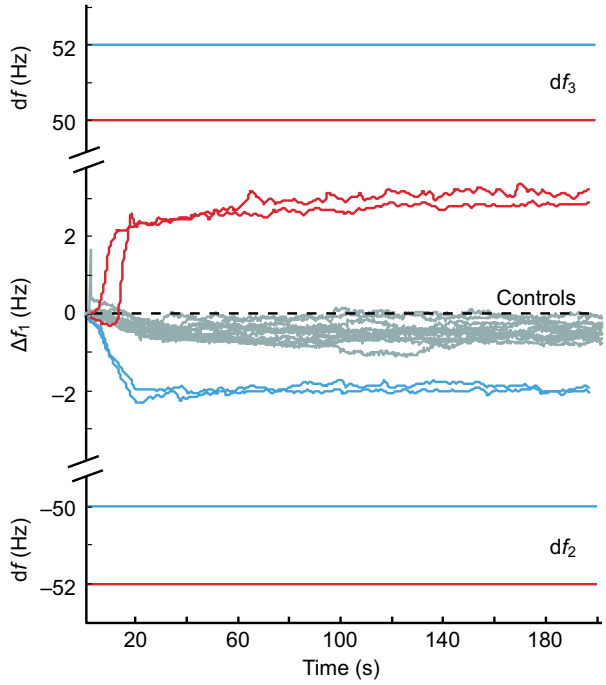

Fig. 4. *Eigenmannia virescens* do not show a change in EOD frequency (Δf_1) when stimulated with a single sinusoid with |d*f*| >50 Hz (control; gray). The fish respond to sums of two sinusoids that contain a low-frequency envelope. Two trial types are shown, where df_2=–50 and df_3=+52 (+2 Hz envelope; blue lines) and where df_2=–52 and df_3=+50 (–2 Hz envelope; red lines). The fish shift their frequency down for positive envelopes (blue trials) and up for negative envelopes (red trials).

not change by more than ±1 Hz for at least 25 consecutive minutes, which typically took 1–3 h.

Trials were presented across multiple testing blocks that lasted 1–3 h and were completed on different days. Between testing sessions the fish was returned to its home tank to reduce changes in response due to motivation, fatigue or other unknown factors. If the EOD responses of the fish deteriorated over the course of testing the fish was placed back in the home tank for 1–5 days and then re-tested.

Experimental setup

The chirp chamber was positioned such that the fish was located in the middle of two electrodes (head-to-tail) separated by 25 cm (Fig. 3, red electrodes), used to record the EOD. All stimuli were applied into the tank *via* transverse electrodes separated by 25 cm with the fish located in the middle (Fig. 3, black electrodes). A 1 cm transverse dipole (Fig. 3, yellow electrodes) adjacent to the head of the fish measured the local electric field, which was used to estimate stimulus amplitude.

At the start of each trial the initial EOD frequency of the fish (f_{1i}) was extracted. All trials within a testing block were presented randomly for each fish. Each trial lasted 200 s with an inter-trial interval of 200 s. For each trial, the fish was presented with a stimulus that was either a single sinusoid (control trials; S_2) or a sum of two sinusoids (envelope trials; S_2+S_3).

For the envelope trials, the frequencies of the individual sinusoids (f_2 and f_3) were calculated by adding a specified initial frequency difference (df_i) to f_{1i}, i.e. f_2=f_{1i}+df_{2i} and f_3=f_{1i}+df_{3i}. For control trials, only f_2 was calculated and applied. The frequencies f_2 and f_3 were held constant, i.e. not clamped to f_1, so changes in the fish's EOD frequency results in changes in the value of each d*f* and the dd*f*.

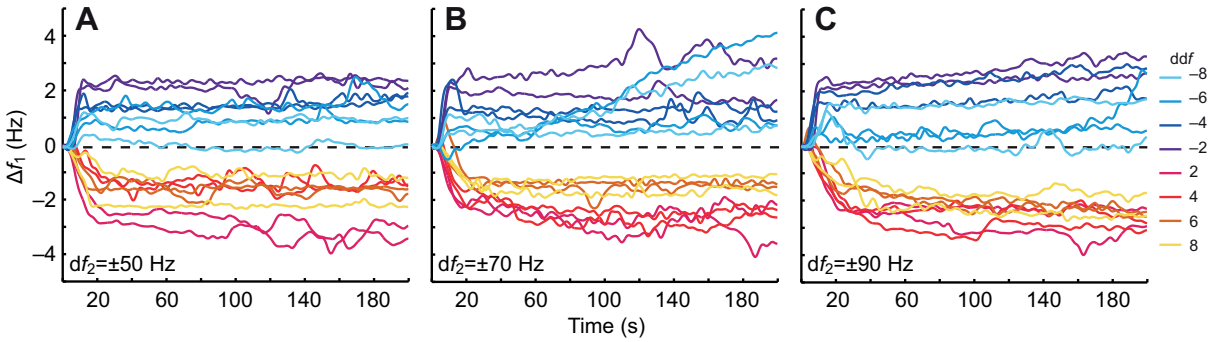

Fig. 5. The Social Envelope Response (SER) is dependent on dd*f* and not d*f*. In each panel, the initial dd*f* was varied from –8 to +8 Hz in 2 Hz intervals (excluding 0). (A) df_2=±50 Hz, (B) df_2=±70 Hz and (C) df_2=±90 Hz. The strength and direction of SER responses was dependent on the dd*f*. In contrast, fish show no systematic differences in responses to dd*f* values as a function of the range of df_2 and df_3 values used.

Experimental stimuli

Control trials

All fish completed trials (N=20) with a single sinusoid stimulus (S_2) at a specified high |d*f*| (>40 Hz). The initial d*f* values used were ±52, 58, 72, 78, 92 and 98 Hz, which are outside the range of frequencies known to elicit the JAR. These d*f* values were a subset of those used to create the envelope stimuli in other trials (see below). For all control trials the stimulus amplitude was 0.74 mV cm^{-1} and the stimulus amplitude ramp time was 20 s.

Amplitude trials

All fish completed trials (N=10), with a sum of two sinusoids (S_2+S_3) that produced a ddf_i of ±4 Hz. The initial d*f* values used were ±48 and ±52, such that there were two trial types: df_{2i}=–48 and df_{3i}=+52 or df_{2i}=–52 and df_{3i}=+48, which resulted in a +4 Hz and a –4 Hz envelope, respectively. These trials were repeated at five different stimulus amplitudes (0.15, 0.45, 0.74, 1.05 and 1.34 mV cm^{-1}) with a ramp time of 20 s.

Envelope trials

All fish completed trials (N=48) with a sum of two sinusoids (S_2+S_3) that produced a specified ddf_i. Trials were completed with df_{2i}=±50, ±70 or ±90 with df_{3i} sweeping from –df_{2i}–8 to –df_{2i}+8 at intervals of 2 Hz. For example, for df_{2i}=50, df_{3i} was set at each of the following values for individual trials: –58, –56, –54 or –52 (resulting in initial dd*f* values of –8, –6, –4 and –2 Hz) or –48, –46, –44 and –42 (resulting in initial |dd*f*| values of 2, 4, 6 and 8 Hz). For trials where df_{2i}=–50, the df_{3i} values were the same as the above example, except with a positive sign. This was repeated for df_{2i}=±70 and ±90, resulting in trials with ddf_i values from –8 to +8 in increments of 2 Hz (excluding 0), produced by d*f* values of varying frequencies. All trials were completed with combined stimulus amplitude of 0.74 mV cm^{-1} and a ramp time of 20 s.

Ramp-time trials

One fish completed trials (N=30) with a sum of two sinusoids (S_1+S_2), where three amplitude ramp times were tested (1, 20 and 100 s). Each ramp time was repeated for two envelope frequencies (+4 Hz: df_{2i}=–48, df_{3i}=+52; and –4 Hz: df_{2i}=–52, df_{3i}=+48) and five stimulus amplitudes (0.15, 0.45, 0.74, 1.05 and 1.34 mV cm^{-1}).

Ratio trials

One fish completed trials (N=10) with a sum of two sinusoids (S_2+S_3), where the relative amplitudes of each individual component were varied at a ratio of 1:1, 1:3, 2:3, 3:2 and 3:1 for envelopes of +4 Hz (df_{2i}=–48, df_{3i}=+52) and –4 Hz (df_{2i}=–52, df_{3i}=+48).

Data analysis

For each trial the recorded EOD was used to compute the EOD frequency as a function of time, $f_1(t)$. This was achieved *via* post-processing with a custom script in MATLAB (MathWorks, Natick MA, USA) that computed the spectrogram of the recorded signal and determined $f_1(t)$ as the frequency with the highest power near the fish's baseline EOD frequency. The baseline f_{1i} was measured at the start of each trial using a frequency-to-voltage (F2V) converter (FV-1400, Ono-Sokki, Yokohama, Japan). For 60 trials the output of the F2V converter was verified against post-experiment Fourier analysis. The error between the two measurements was negligible (mean ± s.d.=0.0008±0.054 Hz). f_1 stabilized by the last 60 s of each trial; f_{1f} is the mean frequency measured over this period. The change in frequency was calculated as $\Delta f_1 = f_{1f} - f_{1i}$.

For each trial, Δf_1 was normalized to the individual fish's maximum response, $|\Delta f_{1max}|$, to allow responses to be compared across fish. Because fish could raise or lower their EOD frequency, some measures are normalized as $|\Delta f_1|/|\Delta f_{1max}|$. Dependent measures were analyzed using one-way repeated-measures ANOVA. For significant main effects, effect size (ηp^2) is given to allow comparison between measures. Additionally, *post hoc* Tukey's honestly significant difference (HSD) tests were run on each significant main effect. We indicate the critical value (Q_{crit}) for each test and provide the obtained values (Q_{obt}) only for those that were statistically significant (i.e. greater than the critical value).

RESULTS

EOD frequency changes were not elicited by high |d*f*| values

To ensure that observed responses were not due to the individual d*f* values, we conducted control trials where fish were presented with a single sinusoid stimulus that had a high |d*f*|. We measured Δf_1 during the last 60 s of the inter-trial interval and found that the EOD frequency was stable without stimulation (mean ±s.e.m.=0.05±0.006 Hz). In addition, Δf_1 across the first 10 s (0.23±0.03 Hz) and the last 60 s (0.52±0.04 Hz) of control stimulus presentation produced only nominal changes to the EOD frequency. Responses to all control trials by a single fish are shown in Fig. 4A. Thus, it is unlikely that the observed Δf_1 to the sum of sinusoid stimuli (which has an emergent envelope) was due to a response to any individual component alone.

Fish exhibited an SER

The sum of two sinusoid stimuli (S_2+S_3) elicited changes in EOD frequency. Fig. 4 shows a characteristic SER of a single fish to two replicates of a +2 Hz envelope (df_2=–50, df_3=+52; blue) and two replicates of a –2 Hz envelope (df_2=–52, df_3=+50; red). The figure shows that the envelope response differs from the response observed to control stimuli (gray).

Across all fish, responses to control stimuli were minimal (range=0.05 to 0.74 Hz) compared with the SERs (range=1 to 4 Hz). Moreover, the time course of EOD change during control trials was much larger than the time course of the SER, which corresponded to the stimulus ramp time (20 s). In addition, responses to control trials were biased downward, while the SERs were bidirectional. The direction of the SER shows that the fish shifts its EOD frequency down when the envelope frequency (dd$f$) is positive and up when the envelope frequency is negative. The direction of the SER was typically opposite the sign of the dd$f$, resulting in the EOD shifting towards the closer df (although the final |df| values were 40 Hz or above).

SER was stronger for lower-frequency envelopes

Fish changed f_1 in response to sum-of-sinusoid stimuli that created initial envelopes in the frequency range of |ddf_i|=2 to 8 Hz as illustrated for a single fish in Fig. 5. The figure also illustrates that Δf_1 is qualitatively similar across all df values used. However, the strength of the SER (the change in EOD frequency during a trial) is dependent upon on |ddf_i| (Fig. 6A). The effect of the initial absolute envelope frequency, |ddf_i|, on the normalized absolute EOD frequency change, $|\Delta f_1|/|\Delta f_{1max}|$, was significant ($F_{3,9}$=6.45, P=0.04, ηp^2=0.68). Normalized $|\Delta f_1|$ is generally smaller as a function of larger initial dd$f$: mean ± s.e.m.=0.59±0.04 for 2 Hz, 0.52±0.03 for 4 Hz, 0.34±0.03 for 6 Hz and 0.39±0.04 for 8 Hz. The only significant pairwise differences (Tukey's HSD, Q_{crit}=4.41) were between the lowest envelope frequency (2 Hz) and those higher than 6 Hz (2 Hz *versus* 6 Hz: Q_{obt}=4.45; 2 Hz *versus* 8 Hz: Q_{obt}=5.51; Fig. 6A, asterisks). The rest of the pairwise comparisons were not significant (Q_{obt}<4.41).

SER increased the envelope frequency

Fish change f_1 in response to initial envelope stimuli, which resulted in a change in the envelope frequency (Fig. 6B). In general, the final absolute envelope frequency settles in the range of 5–15 Hz (mean ± s.e.m.=8.87±0.20 Hz). The change in envelope frequency (Δdd$f$=|ddf_f|–|ddf_i|) as a function of ddf_i is shown in Fig. 6C. We found a significant effect of the initial envelope frequency (|ddf_i|) on the Δdd$f$ ($F_{3,9}$=6.32, P=0.01, ηp^2=0.68) such that the change in envelope frequency, |Δdd$f$|, was smaller as a function of larger |ddf_i|: mean ± s.e.m.=4.78±0.68 for 2 Hz, 4.57±0.51 for 4 Hz, 2.86±0.36 for 6 Hz and 3.29±0.59 for 8 Hz. The only significant pairwise differences (Tukey's HSD, Q_{crit}=4.41) were between 2 and 6 Hz (Q_{obt}=5.05) and between 4 and 6 Hz (Q_{obt}=4.50), where the change in envelope frequency was greater for the lower initial envelope frequency in each pair.

SER depended on stimulus amplitude and not the rate of amplitude change

The strength of the SER, measured by the magnitude $|\Delta f_1|$, increased as a function of stimulus amplitude (shown for one fish in Fig. 7A). The effect of stimulus amplitude on the normalized $|\Delta f_1|$ was significant ($F_{4,12}$=7.16, P=0.02, ηp^2=0.71; Fig. 7B). The change in frequency, $|\Delta f_1|$, was generally larger for larger stimulus amplitudes: mean ± s.e.m.=0.32±0.07 for 0.15 mV cm^{-1}, 0.49±0.09 for 0.45 mV cm^{-1}, 0.68±0.11 for 0.74 mV cm^{-1}, 0.63±0.09 for 1.05 mV cm^{-1} and 0.83±0.06 for 1.34 mV cm^{-1}. There were significant pairwise differences (Tukey's HSD, Q_{crit}=4.21) between the lowest stimulus amplitude (0.15 mV cm^{-1}) and those higher than 0.74 mV cm^{-1} (0.15 *versus* 0.74: Q_{obt}=5.16; 0.15 *versus* 1.05: Q_{obt}=4.49 and 0.15 *versus* 1.34: Q_{obt}=7.20) and between the second lowest stimulus amplitude (0.45 mV cm^{-1}) and the highest stimulus amplitude (0.45 *versus* 1.34: Q_{obt}=4.73; Fig. 7B, asterisks). Other pairwise comparisons were not significant (Q_{obt}<4.20).

The effect of stimulus amplitude on final |ddf_f| was significant ($F_{4,12}$=7.99, P=0.04, ηp^2=0.73; Fig. 7C). There was a significant pairwise difference (Tukey's HSD, Q_{crit}=4.20) between the lowest stimulus amplitude (0.15 mV cm^{-1}) and those higher than 0.74 mV cm^{-1} (0.15 *versus* 0.74: Q_{obt}=5.25; 0.15 *versus* 1.05: Q_{obt}=4.71; and 0.15 *versus* 1.34: Q_{obt}=7.65) and between the second

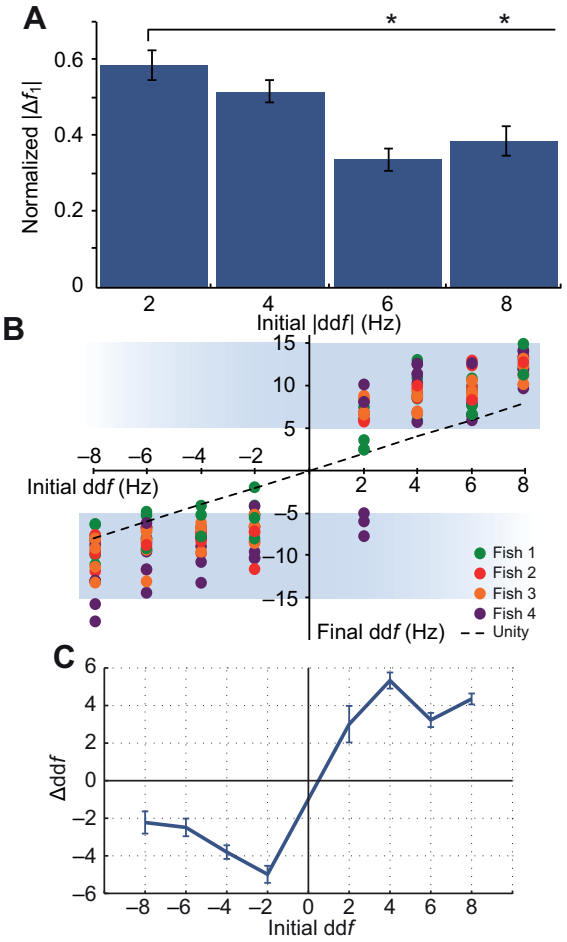

Fig. 6. SER strength as a function of initial dd$f$. (A) Normalized $|\Delta f_1|$ (1 indicates greatest response, 0 indicates lowest response) was significantly greater when the initial |dd$f$| was lower. (B) The f_1 generally shifted in the predicted direction for all fish (colored circles). For most responses, the final envelope frequency was greater than the initial envelope frequency. This is visualized on the plot when the magnitude of the data point is greater than the unity (dashed line). In the three trials that did not go in the predicted direction (purple circles, bottom right), the fish nevertheless increased the envelope by having a stronger response but in the opposite direction. Final |dd$f$| values were typically between 5 and 15 Hz (shaded band). (C) The change in envelope frequency (Δdd$f$=|ddf_f|–|ddf_i|) as a function of ddf_i. The |Δdd$f$| was generally decreased for initial envelopes that were higher in frequency.

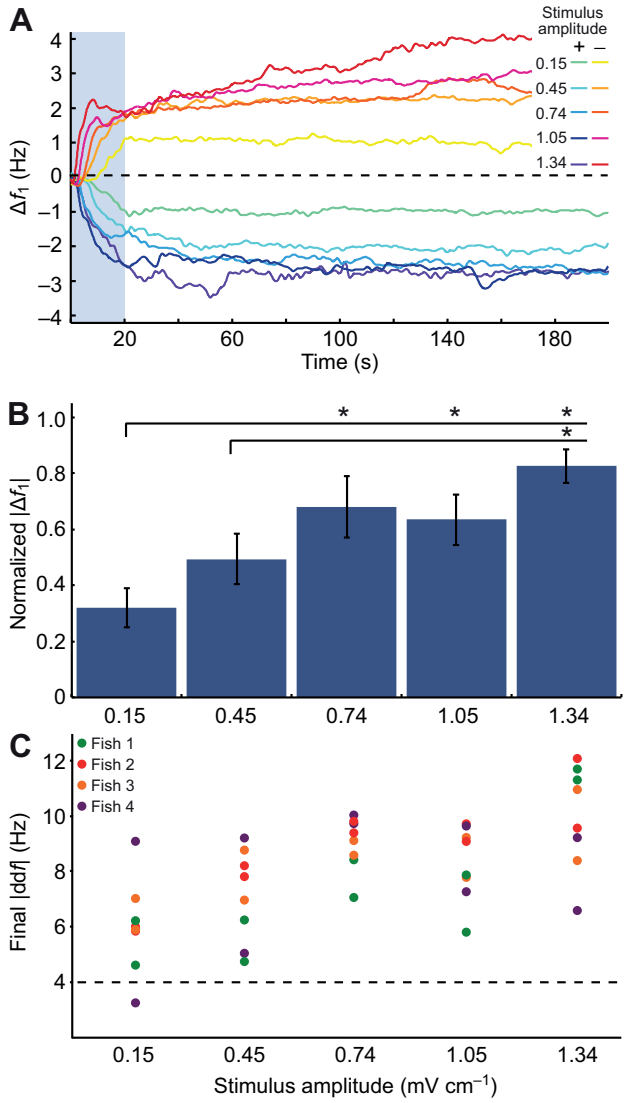

Fig. 7. SER as a function of stimulus amplitude. (A) EOD frequency traces showing that the strength of the Δf_1 increases as the stimulus amplitude was increased from 0.15 to 1.34 mV cm^{-1}. The light blue box indicates the period (ramp time) over which the stimulus amplitude was increased from zero to its final value. (B) There was a significant effect of the stimulus amplitude on the strength of the EOD frequency change where stronger responses were observed for higher stimulus amplitudes. (C) The final |dd*f*| was significantly higher in frequency for larger stimulus amplitudes, across individuals (color-coded).

lowest stimulus amplitude (0.45 mV cm^{-1}) and the highest stimulus amplitude (0.45 *versus* 1.34: Q_{obt}=4.83). Other pairwise comparisons were not significant (Q_{obt}<4.20).

In data from one fish, differences in ramp time did not effect the strength of the SER, $|\Delta f_1|$ (Fig. 8). Thus, the SER strength depended on the amplitude of the stimulus, but not on the rate of change of amplitude.

SER did not switch direction with changes in amplitude ratio

For a given df_2 and df_3 pair, the relative amplitudes of S_2 and S_3 determine the rotation of the 'petals' of the Lissajous but not the general precession. As can be seen for dd*f*=–4 Hz, the petals rotate counter-clockwise for ratios 1:3 and 2:3, and clockwise for 1:1, 3:1 and 3:2, but the graph precesses clockwise in all cases (Fig. 9, top).

Similarly, for dd*f*=+4 Hz the petals rotate clockwise for ratios 3:1 and 3:2 and counter-clockwise for 1:1, 1:3 and 2:3, but the graph precesses counter-clockwise in all cases (Fig. 9, bottom).

We examined the sign of SER, measured by the sign of Δf_1 in response to different stimulus amplitude ratios S_2:S_3 (1:1, 1:3, 2:3, 3:2 and 3:1) for dd*f*=±4 Hz (Fig. 9). We found that the direction of the SER depended only on the sign of dd*f*, not the amplitude ratio; i.e. f_1 shifts up when dd*f* is negative, and f_1 shifts down when dd*f* is positive (Fig. 9, middle). This supports our hypothesis that the SER is driven by the precession of the Lissajous rather than the local rotation of the petals when the d*f* values are outside the JAR range.

DISCUSSION

Forty years of analysis of the JAR (Watanabe and Takeda, 1963; Bullock et al., 1972) have focused on mapping a well-defined computation (Heiligenberg, 1991) through all stages of neural processing, from sensory receptors to motor units (Metzner, 1999). This work was successful mainly due to a sharp focus on the specific parameters that were necessary and sufficient to drive the behavior, thereby putting aside potentially complex temporal features – such as social and movement envelopes – that are likely to be ubiquitous in a fish's electrosensory milieu (Tan et al., 2005; Stamper et al., 2010). Recent neurophysiological studies have identified neurons that respond to such electrosensory envelopes (Middleton et al., 2006; Middleton et al., 2007; Longtin et al., 2008; Savard et al., 2011; McGillivray et al., 2012), but the function of this brain activity was unknown.

Here we show the behavioral relevance of one category of electrosensory envelopes. We measured the EOD responses of *E. virescens* to envelope stimuli like those that would arise from the electrical interactions of three or more motionless conspecifics. We call this behavior the SER. We also proposed a simple extension of the algorithm for the JAR, a low-pass filter of the instantaneous amplitude and phase of the combined signal, which accurately predicts SER behavior.

In the SER, *E. virescens* raised or lowered their EOD frequency, which resulted in an increase in frequency of the envelope by approximately 2–6 Hz, with final envelope frequencies between 5 and 15 Hz. The strength of the SER depended on the initial envelope frequency and the stimulus amplitude: low initial frequencies and high stimulus amplitudes elicited the largest changes in EOD frequency. The SER direction was insensitive to the relative amplitude ratio between stimulus signals, indicating dependence on the slow precession of the Lissajous, as opposed to fast local rotations of the petals, as predicted by our model (see Fig. 9).

Mechanisms for the SER

We extended the widely known model for the control of the JAR with the addition of a low-pass filter that eliminates responses to the local rotations of the Lissajous while retaining its precession. The model does not predict where and how this computation may be implemented in the brain. Part of this computation could be implemented as a saturation nonlinearity of amplitude-coding P-receptors, which would cause them to encode envelopes (Savard et al., 2011). When combined with a rectification circuit in the electrosensory lateral line lobe (ELL) (Middleton et al., 2006; Middleton et al., 2007; Longtin et al., 2008), the amplitude axis of the Lissajous would oscillate at the envelope frequency (Eqn A27). In this case, the phase axis would be filtered independently in downstream circuits to yield the circular Lissajous

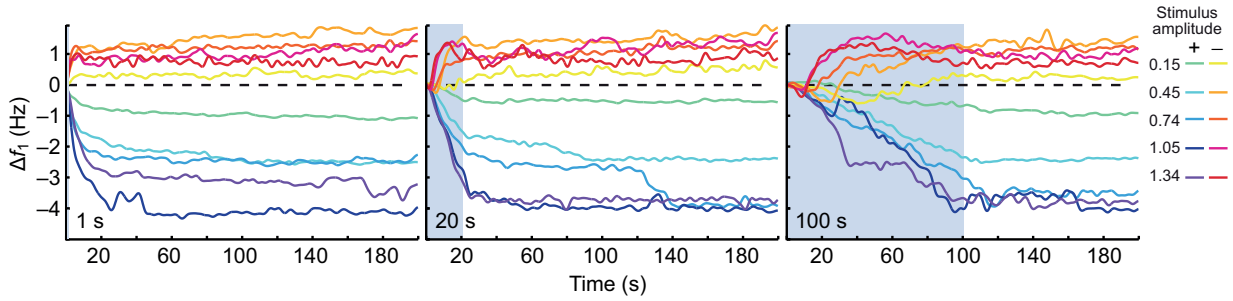

Fig. 8. The strength of the SER was determined by the final stimulus amplitude value and not the rate of change of amplitude. This was observed by comparing data for one individual fish across multiple stimulus amplitude ramp times (1, 20 and 100 s). The initial time course of the behavior increased as the ramp time increased, but the final change in EOD frequency is equivalent across all ramp times.

that precesses at the |dd*f*|. Alternatively, amplitude and phase filtering may both occur in downstream circuits. In this case, the higher response thresholds (as compared with the JAR) may be necessary to overcome the attenuation caused by the filter.

Possible functional relevance of the SER

In their natural habitat, weakly electric fish are commonly found in groups of three or more conspecifics (Tan et al., 2005; Stamper et al., 2010), which is a necessary condition for the SER. We showed that fish exhibited SERs that increased the frequency of envelopes to higher frequencies (up to 15 Hz). The SER appears to be analogous to the JAR, in which fish also shift their EOD frequency, effecting an increase in the frequency of the AM (Heiligenberg, 1991). It has been shown that low-frequency AMs impair aspects of electrolocation and that the JAR may allow fish to avoid this detrimental interference (Heiligenberg, 1973; Bastian, 1987). In addition to the behavioral impairment, it has also been shown that neural responses to moving objects are impaired by low-frequency jamming (Ramcharitar et al., 2005). If the SER functions analogously to the JAR, one would predict that low-frequency envelopes might also degrade electrosensory performance and impair the underlying neural responses to moving objects.

Movement envelopes

Fish are rarely completely motionless; therefore, we expect that movement-related envelopes commonly emerge in groups of two or more fish. These envelopes can encode the relative velocity between fish and possibly provide reliable cues about distance (Yu et al., 2012). We suspect that fish may also exhibit a ‘movement envelope response’ that can be driven by modulations due to the relative movement between individuals. These movement-based envelopes indeed arise in a social context, but for clarity we distinguish them from ‘social envelopes’ as defined in this paper. This distinction is important because social envelopes constitute a special class of signals that arises solely due to the details of the interactions between electric fields of three or more wave-type weakly electric fish. Movement-related envelopes, however, can arise in a variety of contexts, including from non-social sources such as the interaction of fish with objects in their environment.

In the natural habitat, a cacophony of stimuli contribute to modulations of the EOD in *Eigenmannia*, including simple moving objects (Carlson and Kawasaki, 2007), summations of multiple electric signals (as examined in this paper) and movements of nearby electrogenic animals (Metzen et al., 2012). In addition, amplitude and phase modulations influence each other, creating cross

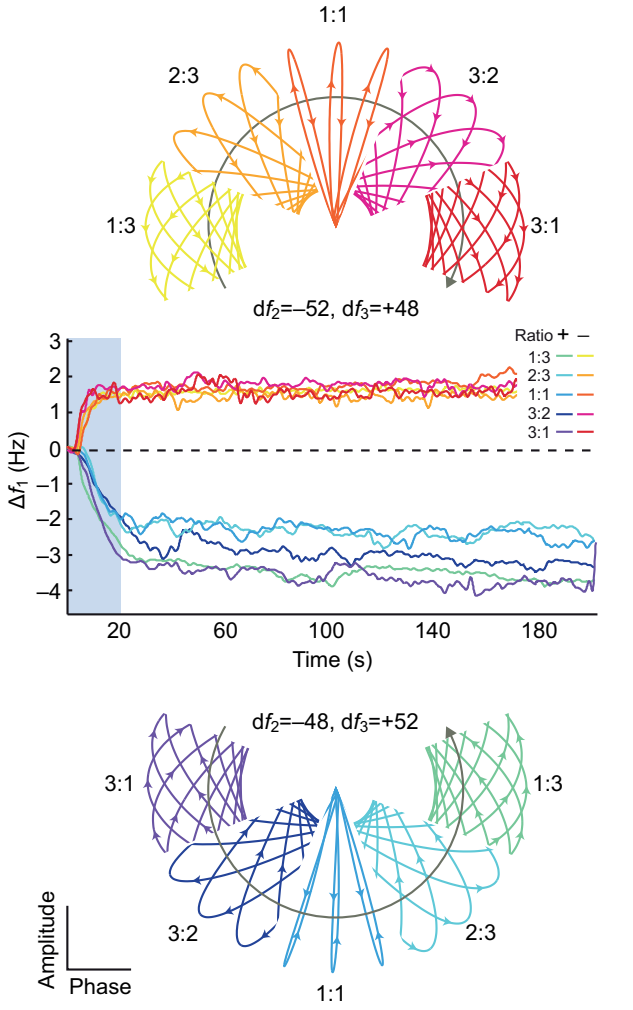

Fig. 9. EOD frequency traces (middle plot) to envelope stimuli (±4 Hz) with different amplitude ratios (S_2:S_2=1:3, 2:3, 1:1, 3:2 and 3:1). The EOD frequency shifts up for negative dd*f* (red spectrum plots) and shifts down for positive dd*f* (blue spectrum plots). The Lissajous figures are representative angular sections of the plots at each of the tested dd*f* values for each amplitude ratio. As the amplitude ratio is varied the direction of the local rotation of the petals can differ from that of the general precession of the Lissajous. The individual ‘petals’ of amplitude ratios 1:3 and 2:3 (negative dd*f*; top) and 3:1 and 3:2 (positive dd*f*; bottom) rotate opposite to the precession (gray arrows). The EOD responses follow the precession and not the local rotations, indicating that they are dependent on dd*f* and not the stimulus amplitude ratio.

interactions, which also have behavioral implications (Carlson, 2008). These and related behaviors appear to be mediated by sets of simple computational rules that are instantiated in the ascending electrosensory pathways of *Eigenmannia* and other closely related species of weakly electric fishes. The behavioral results in this paper provide yet another platform for the analysis and re-analysis of a well-described neural circuit that is used in the control of multiple behaviors.

APPENDIX

This Appendix focuses on social envelopes arising from multiple interacting motionless wave-type weakly electric fish. We address the following questions: (1) what are amplitude modulations and envelopes in the context of interacting EODs; (2) how do AMs and envelopes emerge from sums of sinusoids; and (3) what are the constraints on biological mechanisms for the extraction of AMs and envelopes?

Definition of envelopes

Interactions of the electric fields of two motionless fish with different EOD frequencies give rise to a 'beat' pattern at the $|\mathrm{d}f|$ of the two EOD signals. The sum of two sinusoids can be mathematically decomposed into an amplitude- and phase-modulated signal:

$$a_1\cos(\omega_1 t)+a_2\cos(\omega_2 t)=M(t)\cos(\psi(t))\ . \qquad \text{(A1)}$$

However, the structure of $M(t)$ and $\psi(t)$ is complicated:

$$M(t)=\sqrt{a_1^2+a_2^2+2a_1a_2\cos((\omega_2-\omega_1)t)}\ ,$$

$$\psi(t)=\frac{\omega_1+\omega_2}{2}t+\tan^{-1}\left(\frac{a_1-a_2}{a_1+a_2}\tan\left(\frac{\omega_1-\omega_2}{2}t\right)\right)\ . \qquad \text{(A2)}$$

When $a_1>>a_2>0$, these signals can simplified to an intuitive expression:

$$M(t)\simeq a_1+\frac{a_2}{a_1}\cos((\omega_2-\omega_1)t)\ ,$$

$$\psi(t)\simeq\omega_1 t\ . \qquad \text{(A3)}$$

This holds for electric fish because the self-generated EOD for a fish generally dominates the EODs of conspecifics.

Mathematically, the 'modulator' $M(t)$ above is referred to as the envelope of the signal. However, this quantity is termed an AM by the electric fish community, because envelope coding in electric fish is observed in the afferents of P-type electroreceptors, which code EOD amplitude increases. Thus the source signal for envelope extraction is the AM of the EOD, not the underlying EOD signal itself. We will refer to the envelope of the EOD as the AM, and the envelope of the envelope of the EOD as, simply, the envelope.

For three interacting, motionless EODs (modeled as sinusoids), $M(t)$ and $\psi(t)$ are more complicated. The interactions can produce a combined signal that has higher-order features, such as 'beats of beats' (primarily at the $|\mathrm{dd}f|$), which are termed social envelopes.

The AM $M(t)$ of a signal $s(t)$ is the signal such that, when multiplied by a carrier signal, $\cos\psi(t)$, reproduces $s(t)$, namely $s(t)=M(t)\cos\psi(t)$. Under appropriate assumptions, $M(t)$ is a smooth curve that approximately traces the local maxima of $s(t)$, and $-M(t)$ its minima, and these local extrema approximately correspond to the peaks and troughs of $\cos\psi(t)$. Thus, for an AM to be 'well defined' (in a sense formalized below), the extrema should oscillate at slower frequencies than the carrier. In the case of two sinusoids, the expression for $M(t)$ in Eqn A2 represents a pure AM only if it is in a lower frequency band than the carrier signal $\cos\psi(t)$, i.e. the signals are spectrally separated. In fact the Hilbert transform can be used to decompose such a signal into a product of its amplitude and carrier if those signals are spectrally separated (Bedrosian, 1963; Rihaczek and Bedrosian, 1966). $M(t)$ and $\cos\psi(t)$ resulting from mixing of two sinusoids as in Eqn A2 generally results in infinite harmonics; however, when $a_1>>a_2>0$ and $|\omega_2-\omega_1|<\omega_1$, the majority of the spectral content of the $M(t)$ and $\cos\psi(t)$ is band-separated, so they form well-defined AMs (Lerner, 1960; Rihaczek and Bedrosian, 1966). These restrictions can also be explained in the context of a signal, initially constructed as $s(t)=\hat{M}(t)\cos\hat{\psi}_1(t)$. The AM and carrier extracted by the Hilbert transform, $M(t)$ and $\cos\psi(t)$, will generally not be equal to $\hat{M}(t)$ and $\cos\hat{\psi}_1(t)$ unless $\hat{M}(t)$ and $\cos\hat{\psi}_1(t)$ are themselves band-separated. For three or more sinusoidal EODs, there are analogous constraints on amplitudes and frequencies of the individual EODs in order that their sum produces a well-defined envelope of the AM (see Fig. A1).

Consider a group of N weakly electric fish, assumed to be motionless, with approximated sinusoidal EODs. The EOD of fish k, where $k\in\{1,2,...,N\}$, is perceived at an electroreceptor of fish 1 as $a_k c_k$, where a_k is the amplitude, and $\omega_k=2\pi f_k$ is in radians, where f_k is the frequency of fish k in Hz. a_k is a function of the relative distance and orientation between fish 1 and fish k for $k\neq1$, and a_1

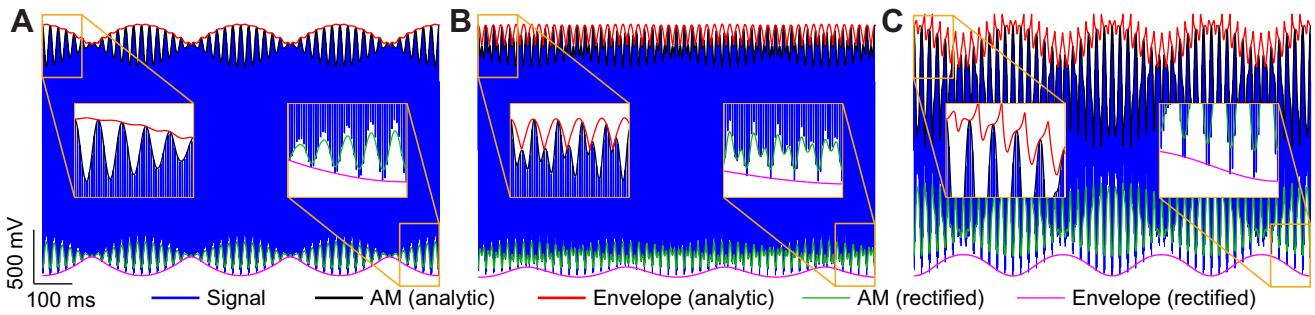

Fig. A1. A sum of three sinusoids (blue), S_1, S_2 and S_3, along with the AM (black) and envelope (red), as calculated from the magnitude of the analytic signal. The AM (green) and envelope (magenta) as calculated from full-wave rectification and filtering are inverted and shifted to the bottom of the combined signal. Enlarged sections of both the top and bottom profiles are shown in each of the plots. f_1 is 500 Hz in all cases. (A) For df at –52 and 48 Hz (with S_1:S_2:S_3 amplitude ratio 10:1:1), the signal has a meaningful envelope at the |dd$f$| at 4 Hz. (B) This is not the case when df values are –48 and 100 Hz, and there is no spectral separation with the |dd$f$| of 52 Hz. The analytic envelope does not follow the amplitude profile of the AMs; here the low-frequency profile is created by a secondary interaction between the |df| at 48 Hz and the |dd$f$| at 52 Hz. The rectification envelope with a low-pass cut-off set at 10 Hz captures this envelope. (C) When the amplitude of S_1 does not dominate (S_1:S_2:S_3 amplitude ratio 5:5:2), the analytic envelope deviates from the extrema of the AM, while the rectified signal produces an 'envelope' in the sense that it tracks some overall structure of the EOD, although the carrier signal is not well defined. It should be noted that the rectification envelope (magenta) in B and C have been amplified; thus this method has the penalty of reduced gain.

would depend on body bending of fish 1. The total signal at the electroreceptor is:

$$s(t)=\sum_{k=1}^{N}a_k\cos(\omega_k t+\phi_k)=\sum_{k=1}^{N}a_k c_k(t)\,, \qquad \text{(A4)}$$

where $\cos(\omega_k t+\phi_k)=\cos(\theta_k)=c_k$. Because $s(t)$ is assumed to be the signal at a receptor of fish 1, the amplitude of fish 1 will generally be greatest, i.e. $a_1>>a_k$, $k=2,3,...,N$.

We have stated that amplitudes and envelopes contain frequencies at the $|df|$ and $|ddf|$ values, but it is clear from Eqn A4 that the signal at the electroreceptor has only components at ω_k. Thus, a nonlinear method is required to extract AMs and envelopes.

Methods for envelope extraction

Magnitude of the analytic signal

A common definition of AMs is as the magnitude of the analytic signal. For a given real input signal $s(t)$, its complex analytic signal is defined as $\mathcal{A}(t)=s(t)+i\hat{s}(t)$, where $\hat{s}$ is obtained by the Hilbert transform:

$$\hat{s}(t)=\mathcal{H}(s)(t)=\frac{1}{\pi}P\int_{-\infty}^{\infty}\frac{s(\tau)}{t-\tau}d\tau=s(t)*\frac{1}{\pi t}\,, \qquad \text{(A5)}$$

where P denotes the Cauchy principal value and * denotes the convolution operator.

There are two key properties of the Hilbert transform used extensively below. First, the Hilbert transform is linear:

$$\mathcal{H}(au(t)+bv(t))=a\mathcal{H}(u(t))+b\mathcal{H}(v(t))\,. \qquad \text{(A6)}$$

Second, the Hilbert transform of sinusoids is given by:

$$\mathcal{H}(\cos(\omega t))=\sin(\omega t)\,,$$
$$\mathcal{H}(\sin(\omega t))=-\cos(\omega t)\,. \qquad \text{(A7)}$$

We can express the analytic signal in polar form as $\mathcal{A}(t)=M(t)e^{i\psi(t)}$. The AM is $M(t)=|\mathcal{A}(t)|$ and the phase function is $\psi(t)=\angle\mathcal{A}(t)$. The nonlinearity in this form of AM extraction arises not from the Hilbert transform or analytic signal construction – which are both linear – but rather from the magnitude operation.

To apply this to the sum of sinusoids signal, let $\mathcal{A}_k$ be the complex analytic signal corresponding to $a_k c_k$, namely $\mathcal{A}_k=a_k c_k+ia_k s_k=a_k e^{i\theta_k}$. Then:

$$\mathcal{A}=\sum_{k=1}^{N}\mathcal{A}_k=\sum_{k=1}^{N}a_k e^{i\theta_k}=M(t)e^{i\psi(t)} \qquad \text{(A8)}$$

is the analytic signal of $s(t)$ in Eqn A4. Graphical representation of this decomposition is shown in Fig. A2, for the three-sinusoid case. The real part of the analytic signal is the real signal $s(t)=M(t)\cos\psi(t)$. The magnitude is calculated *via*:

$$\begin{aligned}M^2(t)&=\left|\sum_{k=1}^{N}a_k e^{i\theta_k}\right|^2=\left(\sum_{k=1}^{N}a_k e^{i\theta_k}\right)\left(\sum_{k=1}^{N}a_k e^{-i\theta_k}\right)\\&=\sum_{k=1}^{N}a_k^2+\sum_{k=1}^{N-1}\sum_{j=k+1}^{N}a_k a_j\left(e^{i(\theta_k-\theta_j)}+e^{-i(\theta_k-\theta_j)}\right)\\&=\sum_{k=1}^{N}a_k^2+2\sum_{k\neq j}a_k a_j c_{k-j}(t)\\&=\alpha^2+2\sum_{k\neq j}a_k a_j(c_{k-j}-1)\,, \qquad \text{(A9)}\end{aligned}$$

where $\Sigma_{k=1}^{N}a_k=\alpha$, and the summation notation $k\neq j$ refers to the $\binom{N}{2}=N(N-1)/2$ combinations of $k,j\in\{1,...,N\}$, $k\neq j$. Hence, we obain the following:

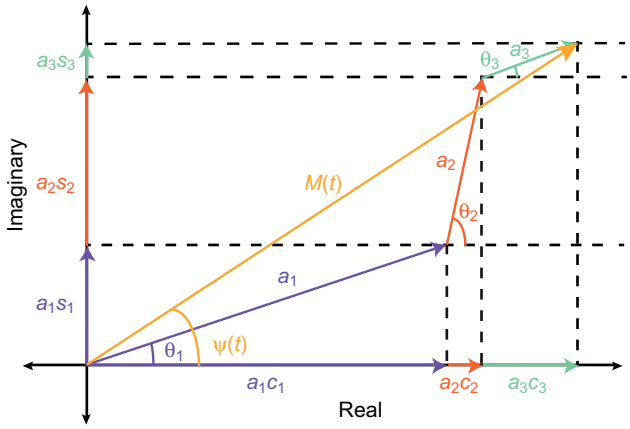

Fig. A2. Analytic representation of sum of cosines signal at time t. Each of the three short vectors represents an analytic signal; the original signals are shown on the 'Real' axis, and their Hilbert transforms on the 'Imaginary' axis. Over time, each vector rotates, tracing a circular path at its angular velocity ω_k. However, because they rotate around the tip of the previous vector, the combined signal (orange vector) traces out a complex Lissajous figure such as in Fig. 2B. This combined signal can be parameterized by the magnitude, $M(t)$, and phase, $\psi(t)$, of the analytic signal.

$$M(t)=\alpha\sqrt{1+\frac{2}{\alpha^2}\sum_{k\neq j}a_k a_j(c_{k-j}-1)}\,. \qquad \text{(A10)}$$

The Taylor series expansion can be first-order approximated as:

$$\sqrt{1+x}=1+\frac{1}{2}x-\frac{1}{8}x^2+\frac{1}{16}x^3+\ldots\simeq 1+\frac{x}{2}\,, \qquad \text{(A11)}$$

when $|x|$ is small. To apply this first-order approximation to Eqn A10, note that:

$$x=\frac{2}{\alpha^2}\sum_{k\neq j}a_k a_j(c_{k-j}-1)\,,0\leq|x|\leq\frac{4}{\alpha^2}\sum_{k\neq j}a_k a_j\,. \qquad \text{(A12)}$$

When a_1 dominates, the upper bound is approximately $4(a_2+...+a_N)/a_1$, which for sufficiently large a_1 is small, and the approximation in Eqn A11 is justified. Thus:

$$\begin{aligned}M(t)&\simeq\alpha+\frac{1}{\alpha}\sum_{k\neq j}a_k a_j(c_{k-j}-1)\\&=\underbrace{\alpha-\frac{1}{\alpha}\sum_{k\neq j}a_k a_j}_{\text{DC}}+\underbrace{\frac{1}{\alpha}\sum_{k\neq j}a_k a_j c_{k-j}}_{\text{d}f/\text{s}}\,. \qquad \text{(A13)}\end{aligned}$$

Subtracting DC, we obtain a 'Hilbert approximation', M_H, of the AM:

$$\begin{aligned}M_H(t)&=\frac{1}{\alpha}\sum_{k\neq j}a_k a_j c_{k-j}\\&=\sum_{k\neq j}b_{kj}\cos((\omega_k-\omega_j)t+(\phi_k-\phi_j))\,, \qquad \text{(A14)}\end{aligned}$$

where $b_{kj}=a_k a_j/\alpha$. The AM is approximately a sum of $\binom{N}{2}$ cosines at the $|df|$ values $|\omega_k-\omega_j|$.

The envelope of this AM is obtained as the magnitude of the analytic signal of the expression in Eqn A14. Repeating steps in Eqns A9 through A14, we obtain:

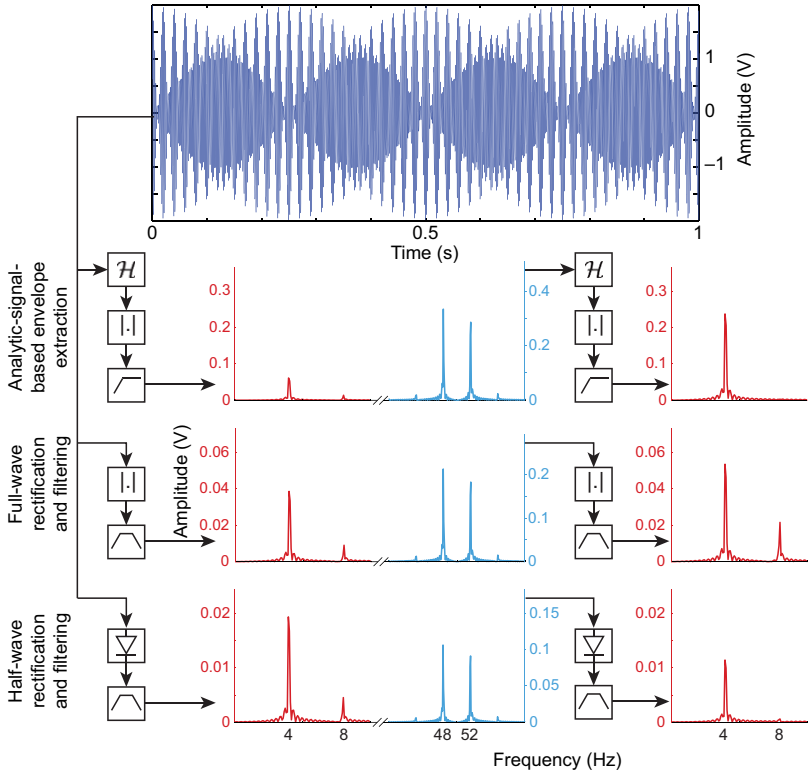

Fig. A3. Envelope extraction methods comparison. The input (top) is the sum of three sinusoids, S_1, S_2 and S_3, at f_1=500, f_2=452 and f_3=552 Hz. S_2 and S_3 had amplitude 0.5, while S_1 had amplitude 1. The first plot in each row is the spectrum of the output of a particular method of envelope extraction, and the second column is the output when the method is used twice in succession. The methods are mnemonically depicted by a sequence of filters, $\mathcal{H}$ depicts extraction *via* the analytic signal, |·| depicts full-wave rectification and the diode depicts half-wave rectification. High-pass and band-pass filters are depicted by frequency response gain functions. It can be seen that all resulting signals from one application of each method have maximum amplitude at the |d*f*| frequencies (48 and 52 Hz), with an additional component at the dd*f* (5 Hz). Applying the method twice extracts out the |dd*f*| component alone. When used twice, each method extracts out the dd*f* component alone, but with varying amplitudes.

$$E_H(t) = \sum e_{kjpq} c_{|k-j|-|p-q|} = \sum e_{kjpq} \cos((|\omega_k - \omega_j| - |\omega_p - \omega_q|)t + (|\phi_k - \phi_j| - |\phi_p - \phi_q|)) , \quad \text{(A15)}$$

where the summation is over the set of all $[N(N^2-1)(N-2)]/8$ combinations of $\{\{k,j\},\{p,q\}\}$ such that $k,j,p,q \in \{1,...,N\}$, $k \neq j$, $p \neq q$, $\{k,j\} \neq \{p,q\}$ and:

$$e_{kjpq} = \frac{b_{kj} b_{pq}}{\beta} = \frac{a_k a_j a_p a_q}{\alpha^2 \beta}, \beta = \sum_{k \neq j} b_{kj} . \quad \text{(A16)}$$

The envelope can be approximated as the sum of sinusoids at |dd*f*| values of the frequencies contained in the original sum of sinusoids. In the context of this paper (mixing of three EODs), from Eqn A15:

$$E_{H3}(t) \simeq \frac{a_1^2 a_2 a_3 \cos(|\Delta\theta_{12}| - |\Delta\theta_{13}|) + a_1 a_2^2 a_3 \cos(|\Delta\theta_{12}| - |\Delta\theta_{23}|) + a_1 a_2 a_3^2 \cos(|\Delta\theta_{23}| - |\Delta\theta_{13}|)}{a_1 a_2 + a_2 a_3 + a_3 a_1} , \quad \text{(A17)}$$

where $\Delta\theta_{12}=(\omega_1-\omega_2)t+(\phi_1-\phi_2)=2\pi(\mathrm{d}f_1)t+(\phi_1-\phi_2)$. Similarly, $\Delta\theta_{13}=2\pi(\mathrm{d}f_2)t+(\phi_1-\phi_3)$ and $\Delta\theta_{23}=2\pi(\mathrm{d}f_3)t+(\phi_2-\phi_3)$. If we assume that $a_1 \gg a_2$ and $a_2 \gg a_3$, we can further approximate this as:

$$E_{H3}(t) \simeq \frac{a_1 a_2 a_3}{a_2 + a_3} \cos(2\pi(\mathrm{dd}f)t + \Phi) , \quad \text{(A18)}$$

where dd*f*=|df_1|−|df_2| and $\Phi=(|\phi_1-\phi_2|-|\phi_1-\phi_3|)$. Thus the envelope is primarily composed of the dd*f*, namely the difference of difference frequencies between fish 1 and other conspecifics.

Caveats of the analytic signal method

Real-time envelope extraction using the analytic signal is not biologically plausible, as the Hilbert transform is a noncausal operator. The analytic envelope of a narrow-band Gaussian white noise, as discussed in Middleton et al. (Middleton et al., 2006), is generally well defined. However, this breaks down as the number of sinusoidal components is reduced (unless one of the amplitudes is dominant), as shown in the case of three EODs in Fig. A1C. The approximation in Eqn A18 is not applicable for a wide range of parameters, e.g. any conspecific amplitude is non-negligible relative to a_1, or insufficient band separation between *f*, d*f* and dd*f*. These limitations do not apply to our experimental setup because: (1) the combined signal perceived by the fish is dominated by its own EOD and (2) the dd*f* and d*f* values used were sufficiently separated.

Envelope extraction *via* rectification and low-pass filtering

A commonly used method of envelope extraction is rectification of the signal followed by filtering. A similar mechanism may be used in electric fish *via* rectification by having the firing threshold of a neuron close to the mean of the input, and then filtering through a slow synapse (Middleton et al., 2007; Longtin et al., 2008).

Full-wave rectification of a zero-mean signal is the absolute value of the signal. For the sum of sines from Eqn A4:

$$|s| = \left|\sum_{k=1}^{N} a_k c_k\right| = \sqrt{\left(\sum_{k=1}^{N} a_k c_k\right)^2} = \sqrt{\sum_{k=1}^{N} a_k^2 \left(\frac{1+c_{2k}}{2}\right) + 2\sum_{k \neq j} a_k a_j \left(\frac{c_{k+j}+c_{k-j}}{2}\right)}$$

$$|s| = \sqrt{\frac{\alpha^2}{2}\left(1 + \frac{1}{\alpha^2}\sum_{k=1}^{N} a_k^2 c_{2k} + \frac{2}{\alpha^2}\sum_{k \neq j} a_k a_j (c_{k+j} + c_{k-j} - 1)\right)} . \quad \text{(A19)}$$

Using the first-order Taylor approximation from Eqn A11, we obtain the following:

$$|s| \simeq \underbrace{\frac{\alpha}{\sqrt{2}} - \frac{1}{\sqrt{2}\alpha}\sum_{k\neq j} a_k a_j}_{\text{DC}} + \underbrace{\frac{1}{\sqrt{2}\alpha}\sum_{k\neq j} a_k a_j c_{k-j}}_{\text{d}f\text{s}} + \underbrace{\frac{1}{\sqrt{2}\alpha}\sum_{k\neq j} a_k a_j c_{k+j} + \frac{1}{2\sqrt{2}\alpha}\sum_{k=1}^{N} a_k^2 c_{2k}}_{\text{Sum frequencies}} \quad . \tag{A20}$$

If the band of difference frequencies $|\omega_k-\omega_j|$ is spectrally separate from that of the sum frequencies $|\omega_k+\omega_j|$, an appropriate filter can extract the df values only, which form the AM. Let $L(\cdot)$ be such a filter, which high-passes DC and low-passes sum frequencies; applying this filter to the rectified signal yields:

$$I_{RF}(t) = L(|s|) \simeq \frac{1}{\sqrt{2}}\sum_{k\neq j} b_{kj} c_{k-j} = \frac{I_H}{\sqrt{2}} \quad . \tag{A21}$$

One more rectification and low-pass filtering step provides us with the envelope, at the |dd$f$|:

$$E_{RF}(t) = \frac{1}{2}\sum e_{kjpq} c_{|k-j|-|p-q|} = \frac{E_H}{2} \quad . \tag{A22}$$

Envelopes extracted by both methods thus have similar spectral content, and the difference frequency components are separated only by scale. Envelopes can also be extracted by half-wave rectification, with qualitatively similar results (see Fig. A3).

The amplitude-phase Lissajous

Here, we explain why the Lissajous figure as described in the paper rotates according to the df values, and why the low-pass filtered version of the Lissajous precesses according to the dd$f$. Consider the summed signal Eqn A4. The phase function $\psi(t)$ is:

$$\psi(t) = \tan^{-1}\frac{\sum a_k s_k}{\sum a_k c_k} \quad . \tag{A23}$$

Using $\tan^{-1}z=(i/2)\{\ln[(1-iz)/(1+iz)]\}$ (where z is a complex number), we have:

$$\psi(t) = \frac{i}{2}\ln\frac{\sum a_k e^{-i\theta_k}}{\sum a_k e^{i\theta_k}} = \theta_1 + \frac{i}{2}\ln\frac{\sum a_k e^{-i(\theta_k-\theta_1)}}{\sum a_k e^{i(\theta_k-\theta_1)}}$$
$$= \theta_1 + \tan^{-1}\frac{\sum a_k s_{k-1}}{\sum a_k c_{k-1}} \quad . \tag{A24}$$

The analytic phase relative to that of fish 1 is:

$$P_L(t) = \psi(t) - \theta_1(t) = \tan^{-1}\frac{\sum a_k s_{k-1}}{\sum a_k c_{k-1}} \quad . \tag{A25}$$

This is the phase of the sum of cosines at the |df| values, $\Sigma_{k=1}^{N} a_k c_{k-1}$. The analytic signal magnitude (Eqn A14), when a_1 dominates, can be further simplified to:

$$M_L(t) = \sum_{k=1}^{N} b_{k1} c_{k-1} \quad . \tag{A26}$$

The Lissajous (M_L *versus* P_L) consists primarily of df components, which is why the graph rotates according to the df values. However, M_L is a first-order Taylor approximation. If, instead, we approximate to the second order, we obtain the following:

$$M_L(t) \simeq \alpha + \frac{1}{\alpha}\sum_{k\neq j} a_k a_j (c_{k-j} - 1) - \frac{1}{2\alpha^3}\left(\sum_{k\neq j} a_k a_j (c_{k-j} - 1)\right)^2 \quad . \tag{A27}$$

The squared term, when expanded, will contain product terms of the form $c_{k-j}c_{p-q}$, which can be written as follows:

$$c_{k-j}c_{p-q} = \frac{1}{2}(c_{|k-j|+|p-q|} + c_{|k-j|-|p-q|}) \quad . \tag{A28}$$

This shows that the amplitude of the analytic signal contains dd$f$ terms $[(a_k a_j a_p a_q)/4\alpha^3]c_{|k-j|-|p-q|}$ (Fig. A3, top). Hence a low-pass filtered version of the Lissajous also serves as a means to extract out components at dd$f$, albeit with reduced magnitudes. Fig. A3 (middle, bottom) shows that a dd$f$ component is also present in the full-wave and half-wave rectified signals. Interestingly, when we apply each extraction method twice in succession, it affects the dd$f$ component differently. It turns out that the half-wave rectified signal contains a stronger component at the dd$f$ than the half-wave rectified AM.

LIST OF SYMBOLS AND ABBREVIATIONS

a_k	amplitude of the kth sinusoid
AM	amplitude modulation
c_k, s_k	$\cos(\theta_k)$, $\sin(\theta_k)$
c_{k-j}, c_{k+j}	$\cos(\theta_k-\theta_j)$, $\cos(\theta_k+\theta_j)$
dd$f$	difference of df values, e.g. $\|df_3\|-\|df_2\|$
df	frequency difference
df_1, df_2, df_3	f_3-f_2, f_2-f_1, f_3-f_1
$E(t)$	envelope of the combined signal
EOD	electric organ discharge
f_1, f_2, f_3	frequencies of S_1, S_2 and S_3, respectively
f_{1f}, df_{2f}, df_{3f}, ddf_f	final values of f_1, df_2, df_3 and dd$f$
f_{1i}, df_{2i}, df_{3i}, ddf_i	initial values of f_1, df_2, df_3 and dd$f$
JAR	Jamming Avoidance Response
$M(t)$	AM of the combined signal
S_1	EOD signal (measured)
S_2, S_3	applied sinusoid signals
SER	Social Envelope Response
t	time
Δf_1	$f_{1f}-f_{1i}$
θ_k	angle (rad) of the kth sinusoid, i.e. $(\omega_k t+\phi_k)$
ϕ_k	phase (rad) of the kth sinusoid
$\psi(t)$	phase modulation of the combined signal
ω_k	frequency (rad s^{-1}) of the kth sinusoid

FUNDING

This material is based on work supported by the National Science Foundation (NSF) [grants IOS-0817918 to E.S.F and N.J.C.; CMMI-0941674 to N.J.C. and E.S.F.; and CISE-0845749 to N.J.C.] and the Office of Naval Research [grant N000140910531 to N.J.C. and E.S.F.]. S.A.S. was supported by an NSF Graduate Research Fellowship.

REFERENCES

Bastian, J. (1987). Electrolocation in the presence of jamming signals: behavior. *J. Comp. Physiol. A* **161**, 811-824.

Bastian, J. and Heiligenberg, W. (1980). Neural correlates of the jamming avoidance response of *Eigenmannia*. *J. Comp. Physiol. A* **136**, 135-152.

Bedrosian, E. (1963). A product theorem for Hilbert transforms. *Proc. IEEE* **51**, 868-869.

Carlson, B. A. (2008). Phantoms in the brain: ambiguous representations of stimulus amplitude and timing in weakly electric fish. *J. Physiol. Paris* **102**, 209-222.

Carlson, B. A. and Kawasaki, M. (2007). Behavioral responses to jamming and 'phantom' jamming stimuli in the weakly electric fish *Eigenmannia*. *J. Comp. Physiol. A* **193**, 927-941.

Heiligenberg, W. (1973). Electrolocation of objects in the electric fish *Eigenmannia*. *J. Comp. Physiol. A* **87**, 137-164.

Heiligenberg, W. (1991). *Neural Nets in Electric Fish*. Cambridge, MA: MIT Press.

Heiligenberg, W. and Bastian, J. (1980). The control of *Eigenmannia*'s pacemaker by distributed evaluation of electroreceptive afferences. *J. Comp. Physiol. A* **136**, 113-133.
Hitschfeld, E. M., Stamper, S. A., Vonderschen, K., Fortune, E. S. and Chacron, M. J. (2009). Effects of restraint and immobilization on electrosensory behaviors of weakly electric fish. *ILAR J.* **50**, 361-372.
Lerner, R. (1960). A matched filter detection system for complicated Doppler shifted signals. *IRE Trans. Inf. Theory* **6**, 373-385.
Longtin, A., Middleton, J. W., Cieniak, J. and Maler, L. (2008). Neural dynamics of envelope coding. *Math. Biosci.* **214**, 87-99.
McGillivray, P., Vonderschen, K., Fortune, E. S. and Chacron, M. J. (2012). Parallel coding of first- and second-order stimulus attributes by midbrain electrosensory neurons. *J. Neurosci.* **32**, 5510-5524.
Metzen, M. G., Fletcher, A. and Chacron, M. J. (2012). Envelope tracking in an active sensory system. *Front. Behav. Neurosci. Conference Abstract: Tenth International Congress of Neuroethology* doi:10.3389/conf.fnbeh.2012.27.00258.
Metzner, W. (1999). Neural circuitry for communication and jamming avoidance in gymnotiform electric fish. *J. Exp. Biol.* **202**, 1365-1375.
Middleton, J. W., Longtin, A., Benda, J. and Maler, L. (2006). The cellular basis for parallel neural transmission of a high-frequency stimulus and its low-frequency envelope. *Proc. Natl. Acad. Sci. USA* **103**, 14596-14601.
Middleton, J. W., Harvey-Girard, E., Maler, L. and Longtin, A. (2007). Envelope gating and noise shaping in populations of noisy neurons. *Phys. Rev. E* **75**, 021918.
Partridge, B. L. and Heiligenberg, W. (1980). Three's a crowd? Predicting *Eigenmannia*'s responses to multiple jamming. *J. Comp. Physiol. A* **136**, 153-164.
Ramcharitar, J. U., Tan, E. W. and Fortune, E. S. (2005). Effects of global electrosensory signals on motion processing in the midbrain of *Eigenmannia*. *J. Comp. Physiol. A* **191**, 865-872.
Rihaczek, A. and Bedrosian, E. (1966). Hilbert transforms and the complex representation of real signals. *Proc. IEEE* **54**, 434-435.
Savard, M., Krahe, R. and Chacron, M. J. (2011). Neural heterogeneities influence envelope and temporal coding at the sensory periphery. *Neuroscience* **172**, 270-284.
Stamper, S. A., Carrera-G, E., Tan, E. W., Fugère, V., Krahe, R. and Fortune, E. S. (2010). Species differences in group size and electrosensory interference in weakly electric fishes: implications for electrosensory processing. *Behav. Brain Res.* **207**, 368-376.
Tan, E. W., Nizar, J. M., Carrera-G, E. and Fortune, E. S. (2005). Electrosensory interference in naturally occurring aggregates of a species of weakly electric fish, *Eigenmannia* virescens. *Behav. Brain Res.* **164**, 83-92.
Watanabe, A. and Takeda, K. (1963). The change of discharge frequency by A.C. stimulus in a weak electric fish. *J. Exp. Biol.* **40**, 57-66.
Yu, N., Hupé, G. J., Garfinkle, C., Lewis, J. E. and Longtin, A. (2012). Coding conspecific identity and motion in the electric sense. *PLOS Comput. Biol.* **8**, e1002564.